An empirical solution for tsunami run-up on compound slopes

Citation	Park, H., Cox, D. T., & Petroff, C. M. (2015). An empirical solution for tsunami run-up on compound slopes. Natural Hazards, 76(3), 1727-1743. doi:10.1007/s11069-014-1568-7
DOI	10.1007/s11069-014-1568-7
Publisher	Springer
Version	Accepted Manuscript
Terms of Use	http://cdss.library.oregonstate.edu/sa-termsofuse

An empirical solution for tsunami run-up on compound slopes

Hyoungsu Park*
Graduate Research Assistant, School of Civil and Construction Engineering, Oregon State University, Corvallis, OR 97331-2302, USA, Email: Hyoungsu.park@gmail.com, Tel: 1-541-602-8618, Fax: 541-737-3052

Daniel T. Cox
Professor, School of Civil and Construction Engineering, Oregon State University, Corvallis, OR 97331-2302, USA, Email: dan.cox@oregonstate.edu

Catherine M. Petroff, Ph.D., P.E.Principal, LP4 Associates LLCAffiliate Faculty, Professional Staff, Dept. of Civil and Env. Engineering, University of Washington

* Corresponding Author

Abstract

Deterministic numerical models for tsunami inundation provide the most accurate means for estimating tsunami run-up when the bathymetry/topography and water level time history at the seaward boundary are well known. However, it is often the case that there is uncertainty in both the bathymetry/topography and water level at the seaward boundary. For these reasons, empirical solutions for tsunami run-up may be preferred because the run-up can be computed quickly allowing a probabilistic estimate the tsunami run-up risk. In this paper,

an empirical solution for tsunami run-up is developed based on an analytic solution and calibrated using a Boussinesq wave model for plane-sloped and compound-sloped cases, including the effects of bottom friction, wave breaking, and the slope of the inundated land area. The new relation is a function of the tsunami wave amplitude at a specific water depth (100 m) to provide clear guidance for practical application, and of two values of the surf-similarity parameter to account for a compound slope. The model comprises three equations for three regions: breaking, transition and non-breaking. The model predictions are compared with survey data from the 2011 Tohoku tsunami in Japan without recalibration. The new equation provides reasonable estimates of run-up height and is generally conservative.

Keywords: Tsunami, Run-up, analytic solution, empirical solution, compound slope, surf-similarity

1. Introduction

Since the 2004 Indian Ocean tsunami, there has been a renewed interest in developing numerical models to estimate tsunami behavior (i.e. generation, propagation and inundation process) including the maximum run-up to define the tsunami hazard zone. However, although there has been rapid improvement in reducing the errors associated with the tsunami propagation and, to a lesser extent, tsunami inundation, there are still significant uncertainties at the generation process to estimate the effects of future tsunamis. Those uncertainties generated from the randomness of nature are often referred to as An aleatory uncertainties (Beven, 2013), and these may be more significant in comparison with epistemic uncertainties which come from the lack of our knowledge (model limitations or limited input).

Generally, numerical models of tsunami run-up are based on depth integrated 2-D (horizontal) or, in limited cases, 3-D models and incorporate horizontal 2-D effects such as diffraction, refraction, reflection and dispersion during the propagation to the near shore, accounting for the complex bathymetry, bottom friction, wave breaking, dissipation, and turbulence during inundation. Even though there are uncertainties due to the gaps between real physics and the existing state-of-art-numerical models, particularly with respect to modeling energy losses during the inundation phase, it is generally true that numerical models provide more accurate results compared to simple analytical or empirical expressions.

However, deterministic numerical models have some limitations with regard to assessing the risk from the tsunami hazard, particularly with respect the aleatory uncertainty at the point of the tsunami generation. This is because deterministic numerical models generally require long computation times, skilled modelers, and detailed input information.

For example, when using a statistical approach to estimate the probable extent of the inundation area, it is necessary to simulate hundreds of scenarios given the uncertainty in predicting the tsunami source, resulting in increased costs and time using numerical models. In addition, the specification of other inputs, including empirical constants to account for surface roughness and other sources of energy loss as well as variations in the tide level, will add to uncertainties of the run-up estimates.

As an alternative to time-dependent tsunami inundation models, analytical or semi-empirical models can provide run-up predictions, and while less precise than time-dependent models for a given scenario, semi-empirical models have an advantage of being computed quickly. Therefore, they can be used in combination with Monte Carlo-type simulations to provide a run-up probability conjoined with the probability of the tsunami source. The basic study of tsunamis started with solving the run-up problem on a beach slope. Carrier & Greenspan (1958) investigated the explicit solution of the non-linear, inviscid shallow water equation on a sloping beach, and Keller & Keller (1964) showed the linear solution of the canonical tsunami run-up problem, that is, a simple uniformly sloped beach with constant depth. Synolakis (1987) used a solitary wave as the tsunami like wave form and provided an analytic solution of a non-linear shallow water wave equation with the simple uniform beach slope condition. Synolakis (1987) noted the importance of classifying the breaking and non-breaking regimes in the experiment data and suggested an empirical run-up solution in the breaking regime based on laboratory experiment data.

Using a wave form composed of a positive solitary wave crest and a negative solitary wave trough, Tadepalli & Synolakis (1994) introduced an analytic solution of positive and negative N-waves which more closely resembles tsunami waves. Kanoğlu & Synolakis (1998) provided an analytic solution on the piecewise linear topographies, and Li & Raichlen (2001) provided an empirically derived correction to Synolakis' analytic solution of the non-linear

shallow water problem in the non-breaking regime. Li & Raichlen (2003) also derived a semi-analytical solution for the breaking regime through an energy balance model. Besides the solitary wave, Carrier, Wu & Yeh (2003) solved a fully nonlinear shallow water equation with Gaussian-type single and N-waves as input conditions, and provided run-up and draw-down motions in physical time and space domain by numerical integration.

Hunt (1959) provided a simple run-up equation for breaking regular waves, where the Iribarren number (surf-similarity parameter) is equal to the ratio of run-up height to deep water wave height (Battjes, 1974). Ahrens & Titus (1985) introduced empirical run-up equations as a function of surf-similarity for regular waves depending on the wave conditions (nonbreaking, plunging, and transitional) and concluded that the regular wave run-up on smooth slopes is largely controlled by surf conditions, slope, and nonlinear effects. Kobayashi & Karjadi (1994) combined numerical model results with laboratory experiments to develop an empirical formula to predict the run-up height normalized by the incident solitary wave amplitude as a function of surf-similarity. Simplified expression of the surf-similarity parameter for solitary waves provided by Fuhrman & Madsen (2008a) while also demonstrating that the parameter functions in a similar way for the run-up of both solitary and period waves. More recently, Lo, Park & Liu (2013) provided empirical run-up formulae with modified forms of the surf-similarity parameter for single and double solitary waves based on experimental data. As an alternative to the surf-similarity parameter, Hughes (2004) suggested the use of a momentum flux parameter to estimate the run-up height for the canonical solitary run-up problem.

Madsen, Fuhrman & Schaffer (2008) questioned using a solitary wave as an initial condition for a tsunami run-up problem since the solitary wave cannot appropriately define the relevant length and time-scales of observed tsunamis. Madsen & Fuhrman (2008) provided maximum run-up and velocity in terms of surf-similarity and amplitude to depth

ratio from the analytic solution of a non-linear shallow water problem at the non-breaking regime, and compared with their Boussinesq type models Fuhrman & Madsen (2008b). Based on this work, Madsen & Schaffer (2010) provided analytic tsunami run-up solutions in terms of the surf-similarity parameter for sinusoidal waves, a single positive wave, N-waves and shoaled linear transient waves in both breaking and non-breaking regimes.

Although the analytical and empirical solutions described above have significantly improved our understanding of tsunami run-up, it can be challenging to apply these formulations in practice. First, there is an ambiguity in input parameters. Several of the previous solutions are based on hydraulic laboratory studies in a wave flume and require knowledge of water depth and wave height at the base of the offshore slope. However, the location of a constant offshore starting depth is uncertain in real applications, and some choices could include the point of wave generation, the edge of a continental shelf, or an arbitrary location that depends on the modeler. Second, existing solutions do not consider compound slopes in part because laboratory studies were often conducted using a plane slope for simplicity and because the analytical treatment of a compound slope is more difficult. In reality, though, the offshore slope (defined here as the slope from the seaward boundary to the shoreline) is often different from the onshore slope (defined here as the slope from the shoreline to the maximum extent of run-up). In general, for the same offshore slope, a milder onshore slope will have a lower run-up than a steeper onshore slope because bottom friction acts over a longer distance for the milder slope and because of the time-dependent nature of the inundation process itself. Finally, previous analytic studies do not include the effects of both wave breaking and bottom friction on the run-up process, factors that cannot be ignored in real tsunami inundation problems.

The purpose of this paper is to provide a new empirical tsunami run-up equation for practical applications. A new set of equations is presented to account for the three factors

described above: well-defined input boundary conditions, compound slopes, and energy loss due to bottom friction and wave breaking. In Section 2, we present the model definitions and a brief review of the analytic solution of Madsen & Schaffer (2010; denoted MS10 hereafter) on which our solution is based. We also apply the Boussinesq model COULWAVE (Lynett et. al., 2002) which we use for model calibration. In Section 3, we present the numerical model estimates of run-up for uniform plane slope and compound slope case studies. First, we test both friction and frictionless conditions with various plane beach slopes and prototype scale tsunami wave input conditions. Second, we test the compound slope (offshore slope and onshore slope) using various wave conditions and describe the slope effects in terms of the surf-similarity parameter. In Section 4, we introduce a new empirical tsunami run-up equation, and review its general characteristics. In Section 5, we present a comparison between the new equations to survey data from the 2011 Tohoku tsunami. In Section 6, we conclude the paper with summary findings, limitations, and recommendations for future work.

2. Definition of parameters

Fig. 1 shows the definition sketch of the one-dimensional tsunami run-up model for this study. Essentially, we use the same canonical 2D run-up problem (Carrier and Greenspan, 1958; Synolakis, 1987; Li and Raichlen, 2001; Carrier et. al., 2003; Madsen and Fuhrman, 2008), but include an additional slope after the shoreline for a compound slope case. The variable h_0 is the flat bottom water depth, and β_1 and β_2 are the offshore slope and onshore slope. When the offshore slope (β_1) and onshore slope (β_2) are equal, the problem reduces to the standard plane slope (β) problem used in MS10 and others. We apply a "single" wave form as defined in MS10 as a tsunami source input time series η given as

$$\eta = A_0 \, \mathrm{sech}^2 (2\pi/T) (t) \qquad \text{Eq. 1}$$

where A_0 is positive tsunami amplitude and T is the representative wave period.

The MS10 study provides analytic run-up solutions for the canonical run-up problem in the non-breaking and breaking regimes. The solutions are

$$R/A_0 = C_1 \xi_1^{2.0} \quad \text{Eq. 2}$$

$$R/A_0 = C_2 \alpha \xi_1^{-0.5} \quad \text{Eq. 3}$$

where R/A_0 is the relative run-up height, and α is $(A_0/h_0)^{-0.25}$. The final relative run-up height is the smaller value between Eq. 2 and Eq. 3. C_1 and C_2 are analytical constants depending on input wave types such as single, N-type, or transient waves. For single wave, $C_1 = 0.1512$ and $C_2 = 4.0513$. Both breaking (Eq.2) and non-breaking (Eq. 3) run-up solutions are functions of the surf-similarity parameter, ξ_1, which is defined as

$$\xi_1 = \tan\beta / (2A_0 / (g T^2 / 2\pi))^{0.5} \quad \text{Eq. 4}$$

where g is the gravitational acceleration, noting that this is the same as the conventional surf-similarity parameter (Battjes, 1974) when $H_0 = 2A_0$. For this paper, we retain the same definition of surf-similarity ξ_1 in Eq. 4 for the offshore slope (β_1) and introduce ξ_2 as the surf-similarity for the onshore slope (β_2) as

$$\xi_2 = \tan\beta_2 / (2A_0 / (g T^2 / 2\pi))^{0.5} \quad \text{Eq. 5}$$

when discussing the compound slope case.

We use the model COULWAVE (Lynett et. al., 2002) as a numerical run-up model. COULWAVE solves a set of Boussinesq equations and includes the effects of bottom friction. A high-order finite-volume numerical solution scheme is employed to solve the conservative-form equations, and the model has been validated through fundamental bench mark problems for the run-up including field data and experiment data (Lynett el. al, 2002; Lynett el. al, 2003; Lynett & Liu, 2005; Park et al, 2013). As a breaking model, COULWAVE applies the eddy viscosity model which is described in Lynett (2006). A common quadratic friction law is applied for the bottom stress term, and the dimensionless friction factor, F, is given as an input value that is constant in both space and time throughout the simulation.

3. Run-up height

3. 1 Run-up height for a plane slope condition

To verify our numerical model setup, we initially compare with the analytic solution of MS10 on a plane slope. For a plane slope comparison, we set $\beta_1 = \beta_2$, and we investigate cases with and without friction. Parameters are selected from the following sets: tan (β) = 1/15, 1/25, 1/50, 1/75, 1/100, 1/150, 1/200, and 1/250; A_0 = 1, 2, and 4 m; and T = 300, 480, 600, and 900 s. The plane slopes varied from a steep (1/15) to a mild slope (1/250) to reflect slopes typically found in nature. In contrast, we found that a majority of laboratory studies of solitary waves on slopes were conducted for fairly steep slopes compared to what is typical in nature. To avoid possible ambiguity in the A_0/h_0 term and to provide some guidance for practical applications, we use a fixed water depth of h_0 = 100 m as this was thought to be a reasonable offshore depth prior to any effects of wave breaking and close enough to the shore to account for effects of refraction and shoaling from the source. In other words, we assume that there is less uncertainty in the tsunami propagation phase from the source to the 100 m depth contour. We calculated a total of 96 combinations with plane slope, amplitude (A_0), and representative period (T), and bottom friction was set to zero (F=0) to allow direct comparison with the work of MS10. To investigate the effect of bottom friction on the solution, we ran an additional 96 cases with F = 0.005, 0.01, and 0.015 using A_0 = 4 m, and the same values tan (β) and T listed above.

The resolution of the model grid was 5 or 10 m, depending on the plane slope (5 m resolution for 1/15, 1/25, and 1/50; 10 m resolution for milder slopes). The length of the numerical wave flume was 90 km and included a sponge layer on the seaward side to eliminate the wave reflections from the open boundary. The projected length of the compound slopes d_1 was 10 km, the length from the slope to the crest of a single wave d_2 was 40 km, and the length of constant depth d_3 was 80 km.

Fig. 2 compares the analytic solution of MS10 and numerical simulation as a function of ξ_1 when $A_0/h_0 = 0.01$ and no friction. The dotted line (from Eq. 3) and cross marked line (from Eq. 2) show R/A_0 at the non-breaking regime and breaking regime, respectively, and the final analytic solution (solid line) is the smaller value of R/A_0 from the two equations. The numerical model results are plotted with different tsunami periods as follows: T = 300 s (circle), 480 s (triangle), 600 s (square), and 900 s (reverse triangle) corresponding to a range of $1.2 < \xi_1 < 42$. According to the analytic solution in Fig. 2 (solid line), the peak point ($\xi_1 \approx 6.0$) is a breaking limit criterion. The relative run-up height (R/A_0) follows the non-breaking run-up solution (Eq. 3) for $\xi_1 > 6.0$, and follows the breaking run-up solution (Eq. 2) for $\xi_1 < 6.0$. In the non-breaking region ($\xi_1 > 6.0$), the numerical results agree well with the analytic solutions (as was demonstrated by MS10) using four different wave periods when $A_0/h_0 = 0.01$, providing confidence in our numerical model setup. However, for $\xi_1 < 6.0$, the results diverge, and the breaking limit criterion of numerical results is closer to $\xi_1 = 2.5$ and not $\xi_1 = 6.0$.

This disagreement for $\xi_1 < 6.0$ originates from a difference between the theoretical breaking criterion and the parameterized breaking in the numerical model. The theoretical breaking criterion is the moment when the Jacobian collapses in the analytic solution; it cannot be utilized to calibrate the numerical model quantitatively at the breaking region because the actual breaking occurs earlier than Jacobian collapse (Synolakis, 1987; Madsen and Fuhrman, 2008). Synolakis (1987) suggested an empirical run-up solution for the breaking regime based on his laboratory data, but it was limited to a single slope of 1:19.85 and the solitary wave condition. Kobayashi & Karjadi (1994) used numerical solutions to the nonlinear shallow water wave equations and experiment data to analyze the run-up problem in the breaking regime and suggested an empirical run-up solution if the surf-similarity is less

than 1.757. However, the solution is only validated from the small range of surf-similarity with limited steep plane slope conditions.

Fig. 3 compares the MS10 analytic solution and numerical model results with friction and without friction where A_0/h_0 is increased to 0.04 (A_0 = 4 m at h_0 = 100 m). In comparing the analytic solution (solid line) to the numerical results with no friction (open symbols), the analytical solution shows a deviation even in the non-breaking region ($\xi_1 > 6$) for A_0/h_0 =0.04. This is likely because of the undulation induced from the sharp transition between the flat bottom and the plane slope (Madsen & Furman, 2008). In addition, the analytical solution relies on the linearity assumption at the toe of the slope, so the deviation between numerical and analytical solutions may increase as A_0/h_0 increases. In comparing the no friction with the friction cases (closed symbols), Fig. 3 shows that without friction, the breaking limit criterion for the analytic solution is about ξ_1 = 6.0, and that for the numerical result was about ξ_1 = 2.5. With friction, the peak shifts to the right, and ξ_1 is almost 10.0. R/A_0 varies noticeably between cases with different friction values. For the breaking region ($\xi_1 < 10$) as the value of friction increases, the relative run-up decreases as expected. For the nonbreaking region ($\xi_1 >$ 10), the frictional effects are less pronounced and the relative run-up is less sensitive to friction values. This implies that reasonable estimates for friction are required especially for the breaking region (mild slopes) rather than nonbreaking region (steep slopes) to estimate the run-up.

3.2 Run-up height for a compound slope

We extend the work of the previous subsection considering a compound slope shown in Fig. 1, using a total of 288 combinations of slopes (β_1 and β_2), amplitude (A_0), and representative period (T). Parameters were selected from the following sets: tan (β_1) = 1/15, 1/50, 1/100, and 1/250; tan (β_2) = 1/15, 1/25, 1/50, 1/75, 1/100, 1/150, 1/200, and 1/250; A_0 = 1.0, 4.0, and 8.0 m; T = 480, 600, and 900 s. As before, the water depth was kept constant at

h_0 = 100 m, and the bottom friction was set as F = 0.01. The resolution of the model grid was 5 or 10 m, depending on β_1 and β_2 (5 m resolution for β_1=1/15 and 1/50 or β_2=1/15, 1/25 and 1/50; 10 m resolution for other cases).

Fig. 4 shows the relative run-up height versus ξ_1 for three relative amplitudes: A_0/h_0 = 0.01 (circle), 0.04 (triangle), and 0.08 (square). The overall trends from plane slope cases with friction in Fig. 3 (solid symbols) are seen again in Fig. 4, and the peak value of R/A_0 occurs around ξ_1 = 8. Some trends can be seen relative to the input value, for example as A_0/h_0 decreases, the relative run-up (R/A_0) generally increases for given ξ_1. However, there is still a large variation in R/A_0 for a given value of ξ_1 due to the compound slope as will be addressed in the next section.

4. Developing a new empirical run-up equation.

To develop a new empirical equation, we started with the basic format of the MS10 analytic solutions that showed good agreement with plane slope numerical model results in the non-breaking regions. In the work of MS10, there was a clear delineation of two regions (breaking and non-breaking) based on ξ_1. For the present compound slope cases with friction and values of A_0/h_0 ranging from 0.01 to 0.08, there appears to be a broader distribution of R/A_0 values near the breaking criterion. Given this, we have designated this region located between the breaking and non-breaking region a 'transition region', located approximately in the range $4 < \xi_1 < 10$. Furthermore, to reflect the effect of a compound slope, we introduce the dimensionless parameter ξ_2 (Eq. 5).

Fig. 5 shows the data of Fig. 4 re-plotted with different symbols to differentiate the onshore conditions. When $\xi_2 < 1.8$ (circle), the corresponding R/A_0 values are roughly less than 2.0, and when ξ_2 is in the range of $1.8 \leq \xi_2 < 4.5$ (triangle), the corresponding R/A_0 values are less than 3.0. When $\xi_2 \geq 4.5$ (square), R/A_0 values are less than 4.0. Each range of

ξ_2 exhibits a threshold value of relative run-up height for each region, and these regions are represented by a single constant variable (γ) in the new empirical equations given by:

$$R/A_0 = C_3 \gamma \xi_1^{0.5} \quad \text{Eq. 6}$$

$$R/A_0 = C_4 \gamma \quad \text{Eq. 7}$$

$$R/A_0 = C_5 \alpha \gamma \xi_1^{-0.5} \quad \text{Eq. 8}$$

$$\gamma = [0.9, 1.2, 1.6] \text{ for } [\xi_2 < 1.8, 1.8 \leq \xi_2 < 4.5, \xi_2 \geq 4.5] \quad \text{Eq. 9}$$

Here, γ is a constant value that depends on the range of ξ_2, and C_3, C_4, and C_5 are empirical constants derived from the numerical results taken as 1.2, 2.5 and 4.0, respectively. The variable $\alpha = (A_0/h_0)^{-0.25}$ is the same as that used in MS10. Eqs. 6, 7, and 8 represent equations for breaking, transition, and non-breaking regions. We did not use the least squares regression for our empirical constant. Instead, we opted for simple values to estimate conservative run-up heights for practical uses. The final form of the new empirical run-up equation is

$$R/A_0 = \text{MIN}\left[(1.2 \gamma \xi_1^{0.5}), (2.5 \gamma), (4.0 \alpha \gamma \xi_1^{-0.5})\right] \quad \text{Eq. 10}$$

where, MIN is the function selecting a minimum value between the three equations and γ is defined by Eq. 9. Fig. 5 shows these new empirical run-up equations (solid lines, Eq. 10) plotted against the numerical model results as a function of surf-similarity parameter ξ_1 for $A_0/h_0 = 0.04$.

Generally, a weak positive correlation between run-up height and ξ_2 is observed: as ξ_2 is increased, R/A_0 also increases, but the value decreases or remains constant in several cases. Thus, we allow ξ_2 to vary as a stepped constant γ rather than a linear parameter in the new empirical run-up equations. Fig. 6 shows the characteristics of the new empirical run-up equation with A_0/h_0 = 0.01, 0.04, and 0.08. R/A_0 is a function of A_0/h_0 only at the non-breaking region. As A_0/h_0 increases, the range of the transition region, the region with constant R/A_0 also increases.

5. Application

In this section, we apply Eqs. 9 and 10 to the 2011 Tohoku tsunami. We use the data from the Nationwide Ocean Wave Information Network for Ports and Harbors (NOWPHAS) GPS buoys as input data and compare calculated relative run-up heights with a subset of the survey data collected from The 2011 Tohoku Earthquake Tsunami Joint Survey Group (TTJS).

The 6 GPS buoys were moored 10 to 20 km offshore and successfully recorded the sea surface elevations as summarized in Table 1 (Kawai et. al., 2012). The water depths at the buoys ranged from $125 < h_{buoy} < 204$ m, the amplitudes of maximum elevations were $2.6 < A_{buoy} < 6.5$ m, and the representative wave periods were between $1000 < T < 1510$ s depending on the buoy location. The representative tsunami period T was determined at each buoy from the elapsed time of a positive wave train exceeding 1% of the maximum amplitude. The corresponding A_{buoy}/h_{buoy} values ranged from 0.019 to 0.040, which is similar to the range of A_0/h_0 used in our new equation. We note that in MS10, A_0/h_0 ranged from 0.00015 to 0.01 which is more indicative of wave conditions in deeper water, such as near the wave source.

Fig. 7 shows the geographic locations of the 6 GPS buoys (GB807, GB804, GB802, GB803, GB806, and GB801), the location of the $h_0 = 100$ m contour, the seven study sites located to the west of the buoys, and positions of the run-up surveys. The run-up data of 2011 Tohoku tsunami were conducted by joint research groups comprising 299 tsunami, coastal, seismology, and geology researchers from 64 universities and institutes throughout Japan (The 2011 Tohoku Earthquake Tsunami Joint Survey Group, 2011, Mori, et. al., 2011, Mori, Takahashi, and TTJS, 2012). The text file of surveyed data was available from the 2011 Tohoku Earthquake Tsunami Joint Survey Group, released 2012-03-30, at http://www.coastal.jp/ttjt/ and provided the location of the end of the run-up points in terms of longitude and latitude, various run-up heights depend on the filtering methods, and

distances from shoreline to run-up points. The provided run-up distances and run-up heights allow for calculated ξ_2 values using run-up corrected from the local MSL. In other words, we assume a plane slope from the shoreline to the run-up point and ignore topographic features in between. Lastly, the survey run-up height data are classified with four reliability levels, and we use only the higher ranked reliability data (2163 points from highly ranked two levels), and these data are presented in Fig. 7 as dots along the eastern coastline from 36.5°N to 40.5°N.

In Fig. 7, we select seven comparison regions (A to G) based on the close proximity to the buoys. One exception is region F which was included because of the significant difference in the onshore slopes relative to the other regions. Positive wave height for each region is calculated at the 100 m water contour line based on the GPS buoy data and linear shoaling excluding effects of wave refraction. Table 2 presents the detailed input information used in the comparisons. A_0 is the positive wave height at 100 m water depth, $Dist_1$ is the average horizontal distance from the 100 m depth point to the shoreline, and $Dist_2$ is the average horizontal distance from the shoreline to the end of the run-up point. Note that we calculate $Dist_1$ and $Dist_2$ for each run-up point, and the average distances are not used in the comparison. A total of 233 run-up points are included in the seven delineated regions.

We present four representative regions (B, E, F, and G) in detail in Figs. 8, 9, 10, and 11. The mean values of ξ_1 for each region (B, E, F, and G) are 11, 3, 1, and 6 respectively (Table. 2), and these values correspond to the three new sub-equations we suggest for the non-breaking (B), breaking (E & F), and transition (G) region. For each of the figures, panel (a) shows a map of the coastline, area of detail, run-up survey location, 100 m contour, and location of the seaward boundary (solid circle). Panel (b) shows the observed relative runup heights (solid) and predicted (open) versus latitude. Panel (c) plots the corresponding distributions of ξ_1 (square) and ξ_2 (triangle) versus latitude.

Fig. 8 shows Region B, on the Omoe Peninsula, near Miyako, corresponding to GB804 which recorded A_{buoy} = 6.5 m and T = 1100 s in a depth of h_{buoy} = 200 m (Table 1). The corresponding shoaled amplitude at h_0 = 100 m water depth was A_0 = 7.7 m, which gives A_0/h_0 = 0.077. The observed run-up varied $2.0 < R/A_0 < 3.7$, while calculated results were generally $R/A_0 = 4.0$, which would be conservative. Fig 8c shows that ξ_1 = 11 and controls the predicted run-up value even though ξ_2 values vary from 40 to 300. This is due to the large value of A_0/h_0 = 0.077 (see Fig 6, thin lines for A_0/h_0 = 0.08).

Fig. 9 evaluates the model performance in Region E which lies near Onagawa along the ria coast and has a complex shoreline, testing the 2D assumption used to derive and calibrate the equation. In this region, the buoy observed A_{buoy} = 5.8 m and T = 1400 s in a depth of h_{buoy} = 144 m. At the 100 m offshore boundary, A_0/h_0 = 0.064. Figure 9b shows that model is generally conservative with R/A_0 in the range $2.5 < R/A_0 < 3.4$ and the observations falling at or below these values in the range $1.0 < R/A_0 < 3.2$.

Fig. 10 evaluates the model for Region F along the Sendai plain which has a much flatter onshore slope and is markedly different from the other regions. We estimated that the amplitude at the h_0 = 100 m contour was A = 4.6 m based on the observations of GB801 and GB806. Fig 10b shows that the compound slope equations predict the run-up reasonably well and are generally conservative. The predicted run-up is generally $R/A_0 = 1.1$ except for some values in the latitude ranging from 38.37 to 38.29 degrees. Here, the predicted values increase to $R/A_0 = 2.2$ consistent with several of the observations. Fig. 10c shows that the offshore value of ξ_1 remains nearly constant in this region, and the increases in R/A_0 are due to the variations in the onshore slope seen in the values of ξ_2 of Fig. 10c.

Fig. 11 evaluates the model performance in Region G which lies near Iwaki and represent the transition region of the model. In this region, the buoy observed A_{buoy} = 2.6 m, T = 1250 s in a depth of h_{buoy} = 137 m. At the 100 m offshore boundary, A_0/h_0 = 0.028 based

374 on the observations of GB806. Fig. 11b shows that the model is generally conservative with
375 R/A_0 in the range $2.3 < R/A_0 < 4.0$ while the observed R/A_0 is in the range $0.8 < R/A_0 < 3.5$.
376 Fig 11c shows that ξ_1 remains mostly constant with a value of 8.0.

377 The measured and predicted run-up heights are compared Fig. 12 for all 7 regions
378 without normalization by the offshore amplitude. The dots comprise all of the surveyed run-
379 up height data from Fig. 7, and cross marks illustrate the data used in the comparison (i.e.,
380 locations A - G). The open circles are the calculated results using the new equations estimates
381 of the local tsunami and slope information (Table 1 and Table 2). The surveyed run-up
382 heights were scattered from almost zero to 40 m depending on the location. Note that in the
383 area around 39.6 ˚N the survey data exhibits a large range of values. This wide variation may
384 result from the complex local geophysical conditions or macro-roughness (i.e. vegetation,
385 harbor infrastructures, or structures) effects which our model could not include at the
386 inundation region.

387 **6. Conclusion**

388 This paper introduces an empirical tsunami run-up equation that includes the effects
389 of bottom friction, wave breaking, and compound beach slopes. The new equation defines
390 tsunami input wave conditions at the 100 m contour and employs a set of three equations that
391 depend on the surf-similarity (Iribarren number). The format of the new equation originates
392 from the run-up solution of MS10, and it includes a parameterization to account for the
393 onshore slope and for the transition between breaking and non-breaking regions. The
394 equations were calibrated using a time-dependent numerical model including the effects of
395 bottom friction. We compared our model without recalibration to the observed run-up data
396 from the 2011 Tohoku Tsunami using shoaled observed buoy data as input. Our model
397 compares well to the observed data and is generally conservative.

The new empirical equation is not applicable for extremely small amplitude or large amplitude waves (much greater than 8 m or less than 1 m), and may not be suitable for complex geophysical conditions (e.g., around headlands, in narrow bays or with effects of coastal structures). For this study we used a single positive wave that follows a sech2 shape as in MS10 and a single general friction coefficient. Future research may include the effect of different types of wave or varying friction coefficients depending on the local inundation circumstances (vegetation or dense urban area). The new equation may be applicable to stochastic approaches for estimating the tsunami inundation hazard when the tsunami source is uncertain. This equation may also useful be for preliminary run-up height estimates without detailed geophysical information for practical engineering problems.

Acknowledgement

This research is based upon work partially supported by the National Science Foundation under Grant No. 0830378 and Oregon Sea Grant under Award No. NB223X. Any opinion, findings, and conclusions or recommendations expressed in this document are those of the authors and do not necessarily reflect the views of the National Science Foundation or Oregon Sea Grant. The authors thank two anonymous reviewers for their constructive comments.

6.1 References

Ahrens, J. P., & Titus, M. F. (1985) Wave run-up formulas for smooth slopes. Journal of Waterway, Port, Coastal, and Ocean Engineering, 111(1), 128-133.

Battjes, J. A. (1974) Surf similarity. In Proceedings of the Fourteenth International Coastal Engineering Conference, vol. 1, pp. 466–480. ASCE.

Beven, K. (2013) So how much of your error is epistemic? Lessons from Japan and Italy. Hydrological Processes, 27(11), 1677-1680.

Carrier, G.F., Greenspan, H. P (1958) Water waves of finite amplitude on a sloping beach. Journal of Fluid Mechanics 17, 97–110.

Carrier, G. F., Wu, T. T. & Yeh, H. (2003) Tsunami run-up and drawdown on a plane beach, J. Fluid Mech. 475, 79–99.

Fuhrman, D. R. & Madsen, P. A. (2008a) Surf similarity and solitary wave run-up. J. Waterway, Port, Coastal, Ocean Eng. 134, 195-198.

Fuhrman, D. R. & Madsen, P. A. (2008b) Simulation of nonlinear wave run-up with a high-order Boussinesq model. Coast. Eng. 55 (2), 139–154.

Hughes, A. S. (2004) Estimation of wave run-up on smooth, impermeable slopes using the wave momentum flux parameter, Coast. Eng. 51, 1085-1104.

Hunt, I. A. (1959) Design of Seawalls and Breakwaters, Journal of Waterway Harbors Division, ASCE, WW3, 123–152.

Kanoğlu, U. & Synolakis, C. E. (1998) Long wave run-up on piecewise linear topographies. J. Fluid Mech. 374, 1–28.

Kanoğlu, U. (2004) Nonlinear evolution and run-up-rundown of long waves over a sloping beach. J. Fluid Mech. 513, 363–372.

Kawai, H., Satoh, M., Kawaguchi, K., & Seki, K. (2012) Recent Tsunamis observed by GPS buoys off the Pacific coast of Japan. Coastal Engineering Proceedings, 1(33), currents.1

441 Keller, J. B., & Keller, H. B. (1964) Water wave run-up on a beach. Research Report NONR-
442 3828(00), Office of Naval Research, Department of the Navy, Washington, DC, 41 p.
443 Kobayashi, N. & Karjadi, E. A. (1994) Surf-similarity parameter for breaking solitary wave
444 run-up. Journal of Waterway, Port, Coastal, and Ocean Engineering 120, 645–650.
445 Li, Y. & Raichlen, F (2001) Solitary wave run-up on plane slopes. J. Waterway Port Coast.
446 Ocean Eng. 127 (1), 33–44.
447 Li, Y. & Raichlen, F (2003) Energy balance model for breaking solitary wave run-up. J.
448 Waterway Port Coast. Ocean Eng. 47, 47–59.
449 Lo, H. Y., Park, Y. S., & Liu, P. L.-F. (2013) On the run-up and back-wash processes of
450 single and double solitary waves-An experimental study. Coastal Engineering, 80, 1-14.
451 Lynett, P., Borrero, J., Liu, P. L.-F., and Synolakis, C. E. (2003) Field Survey and Numerical
452 Simulations: A Review of the 1998 Papua New Guinea Tsunami. Pure and Applied
453 Geophysics, v.160, p. 2119-2146.
454 Lynett, P. and Liu, P. L.-F. (2005) A Numerical Study of the Runup Generated by Three-
455 Dimensional Landslides. JGR-Oceans, v. 110, C03006, doi:10.1029/2004JC002443.
456 Lynett, P., Wu, T., and Liu, P. L.-F. (2002) Modeling wave run-up with depth-integrated
457 equations. Coastal Engineering 46: 89-107.
458 Lynett, P. (2006) Nearshore modeling high-order Boussinesq equations, Journal of Waterway,
459 Port, Coastal, and Ocean Engineering (ASCE), v. 132(5), 348-357.
460 Madsen, P. A. & Fuhrman, D. R. (2008) Runup of tsunamis and long waves in terms of surf-
461 similarity. Coast. Eng. 55 (3), 209–224.
462 Madsen, P. A., Fuhrman, D. R., Schaffer, H. A (2008) On the solitary wave paradigm for
463 tsunamis. J. Geophys. Res. 113, C12012, 1–22.
464 Madsen, P. A. & Schaffer, H. A. (2010) Analytical solutions for tsunami run-up on a plane
465 beach: single waves, N-waves and transient waves. J. Fluid Mech. 645, 27–57.

466 Mori, N., Takahashi, T., Yasuda, T. and Yanagisawa, H. (2011) Survey of 2011 Tohoku
467 earthquake tsunami inundation and run-up, Geophysical Research Letters, 38, L00G14,
468 doi:10.1029/2011 GL049210.
469 Mori, N., Takahashi, T. and The 2011 Tohoku Earthquake Tsunami Joint Survey Group
470 (2012) Nationwide Post Event Survey and Analysis of the 2011 Tohoku Earthquake
471 Tsunami, Coastal Engineering Journal, Vol.54, Issue 4, 1250001, 27p.
472 Park, H., Cox, D. T., Lynett, P., Wiebe, D. M., & Shin, S. (2013) Tsunami inundation
473 modeling in constructed environments: A physical and numerical comparison of free-
474 surface elevation, velocity, and momentum flux. *Coastal Engineering*, *79*, 9-21.
475 Synolakis, C. E. (1987) The run-up of solitary waves. J. Fluid Mech. 185, 523–545.
476 Tadepalli, S. & Synolakis, C. E. (1994) The run-up of N-waves on sloping beaches. Proc. R.
477 Soc. Lond. A 445, 99–112.
478 The 2011 Tohoku Earthquake Tsunami Joint Survey Group (2011) Nationwide Field Survey
479 of the 2011 Off the Pacific Coast of Tohoku Earthquake Tsunami, Journal of Japan
480 Society of Civil Engineers, Series B, Vol. 67 (2011), 1, 63-66.
481

482 **Nomenclature**

Symbol	Descriptions	Unit
A_0	Tsunami wave amplitude	L
d_1	Distance from the slope to the end of the land	L
d_2	Distance from the slope to the center of the tsunami wave	L
d_3	Distance from the slope to the end of the model	L
$Dist_1$	Averaging distance from 100 m contour to shoreline	L
$Dist_2$	Averaging distance from shoreline to end of run-up point	L
F	Friction factor	-
g	Acceleration of gravity	L/T^2
H_0	Wave height	L
h_0	Water depth at the flat bottom	L
MIN	Minimum value	-
R	Tsunami run-up height	L
STD	Standard deviation	-
T	Representative wave period	T
SWL	Still water level	-
β_1	Offshore slope	-
β_2	Onshore slope	-
γ	Empirical coefficient dependent on ξ_2	-
η	Surface elevation	L
ξ_1	Surf-similarity (Irribaren number) for offshore slope	-
ξ_2	Surf-similarity for onshore slope	-

483

List of Figures

509 Fig. 8. Run-up height comparison results for Region B. (a) Coastline map with 100 m water
510 contour (thin line), location of 100 m water depth for model input (solid circle), and
511 GPS buoy location (solid square). (b) Comparison of the relative run-up heights from
512 the survey (solid circle) and the new equation (open circle). (c) ξ_1 and ξ_2 values
513 (open squares and solid triangles).

514 Fig. 9. Run-up height comparison results for Region E. Symbols are same as Fig. 8.

515 Fig. 10. Run-up height comparison results for Region F. Symbols are same as Fig. 8.

516 Fig. 11. Run-up height comparison results for Region G. Symbols are same as Fig. 8.

517 Fig. 12. Total surveyed run-up heights (dots) along the coastline from 36.5˚N to 41˚N,
518 surveyed data used for comparison (cross marks), and corresponding Eq. 11
519 estimates (open circles).

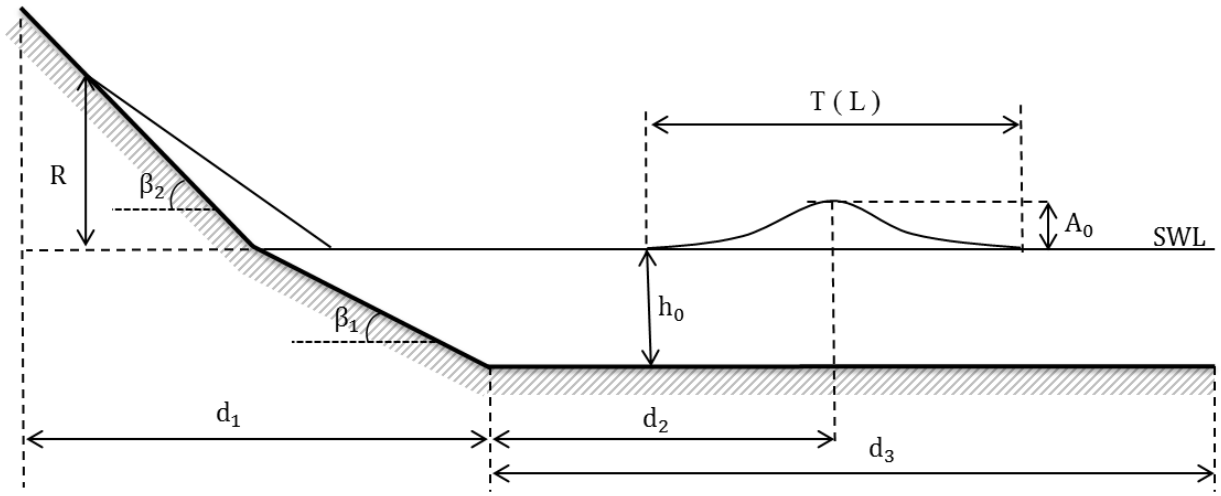

Fig. 1: Sketch of the tsunami run-up height model bathymetry and setup for the compound slope condition. Offshore slope is β_1 and onshore slope is β_2.

524

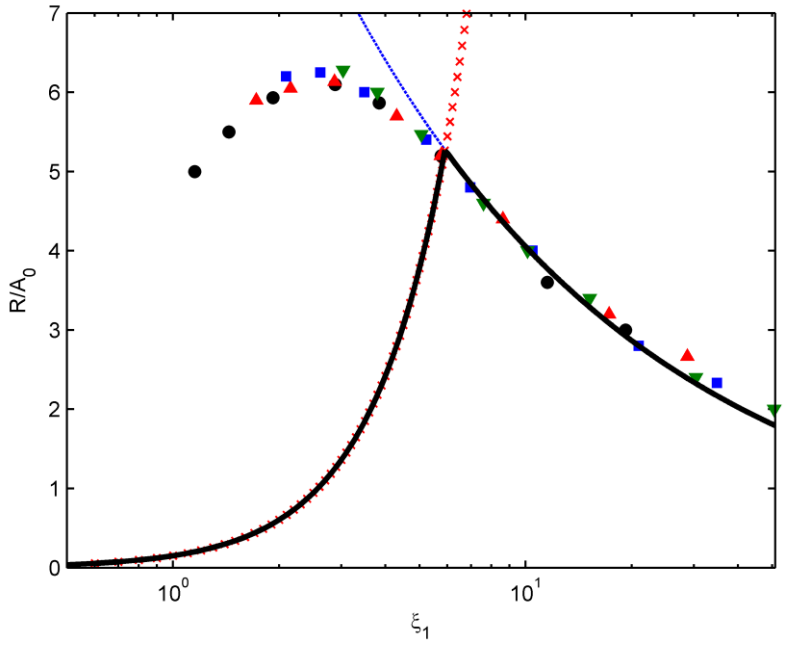

525

526 Fig. 2: Comparison between the dimensionless maximum run-up height for single wave,
527 A_0/h_0 = 0.01, of Madsen and Schaffer (2010) analytic solution (thick black solid line) and
528 numerical model (COULWAVE) results (solid symbols) as a function of the surf-similarity
529 defined by Madsen and Schaffer (2010). The dotted line is an analytic solution of Madsen
530 and Schaffer (2010) at the non-breaking regime and x marked line is at the breaking regime.
531 Each symbol represents different tsunami periods; T=300 s (circle), T=480 s (triangle),
532 T=600 s (square), and T=900 s (inverse triangle).

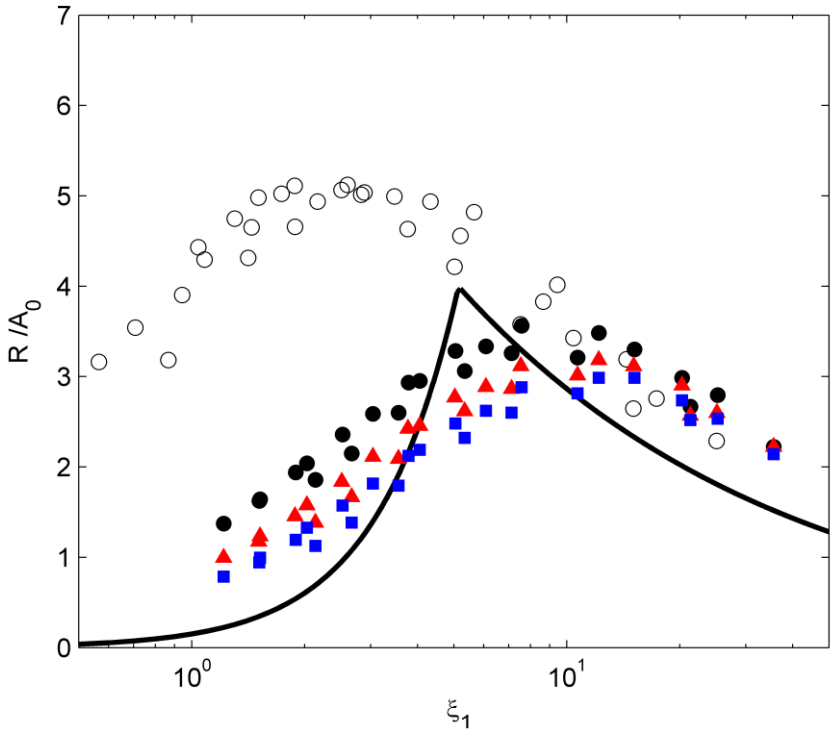

533

534 Fig. 3: Comparison between Madsen & Schaffer (2010) single wave analytic solution and
535 Numerical model (COULWAVE) results with various friction values; F=0 (open circle),
536 F=0.005 (solid circles), 0.01 (solid triangles) and 0.015 (solid squares). A_0/h_0 = 0.04.

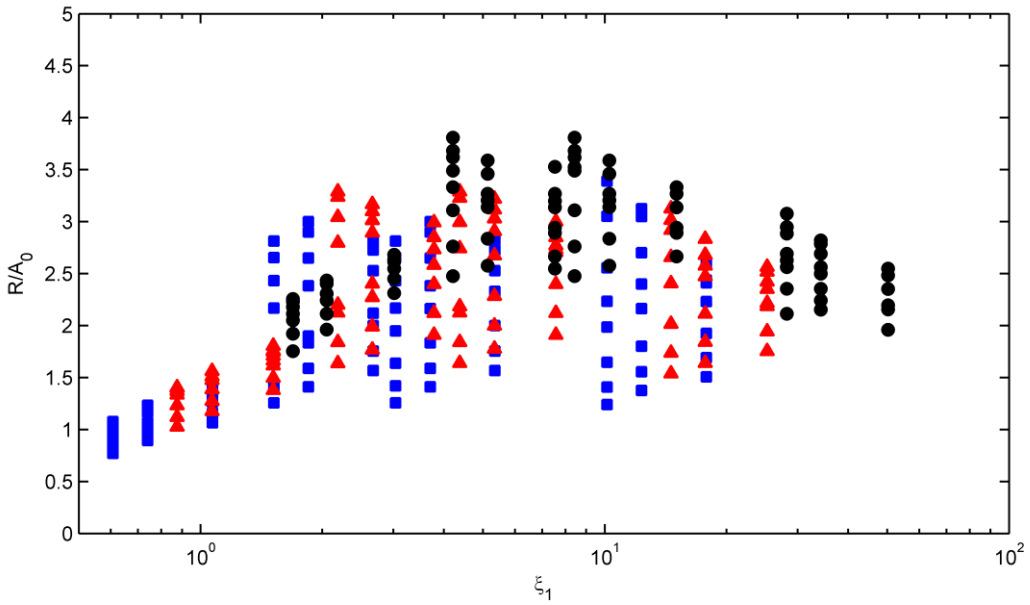

Fig. 4: Relative run-up height from compound slope numerical model results as a function of the surf-similarity parameter (ξ_1) with various amplitudes (A_0); A_0/h_0 = 0.01 (solid circles), A_0/h_0 = 0.04 (solid triangles), and A_0/h_0 = 0.08 (solid squares).

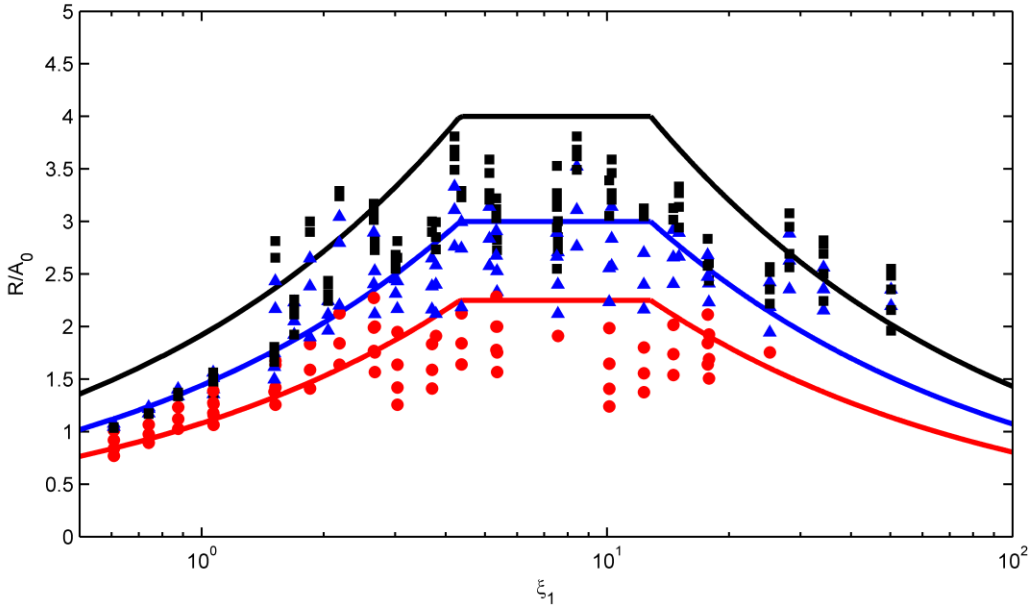

Fig. 5. Eq. 10 (solid lines) for $A_0/h_0 = 0.04$, and numerical model results (symbols) classified by onshore surf-similarity (ξ_2) as follows: $\xi_2 < 1.8$ (bottom line, circles), $1.8 \leq \xi_2 < 4.5$ (middle line, triangles), and $\xi_2 \geq 4.5$ (top line, squares).

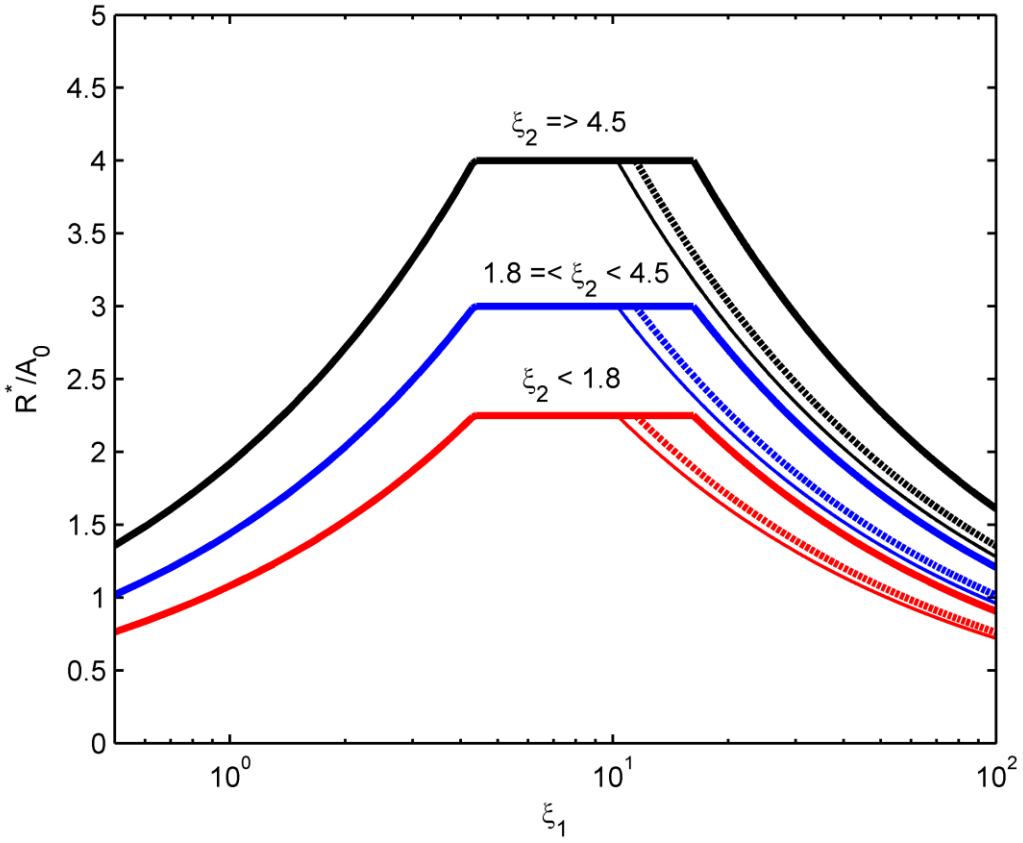

Fig. 6: Eq. 10 with A_0/h_0 of 0.01 (thick), 0.04 (dotted), and 0.08 (thin) for $\xi_2 < 1.8$ (bottom lines), $1.8 \leq \xi_2 < 4.5$ (middle lines), and $\xi_2 \geq 4.5$ (top lines).

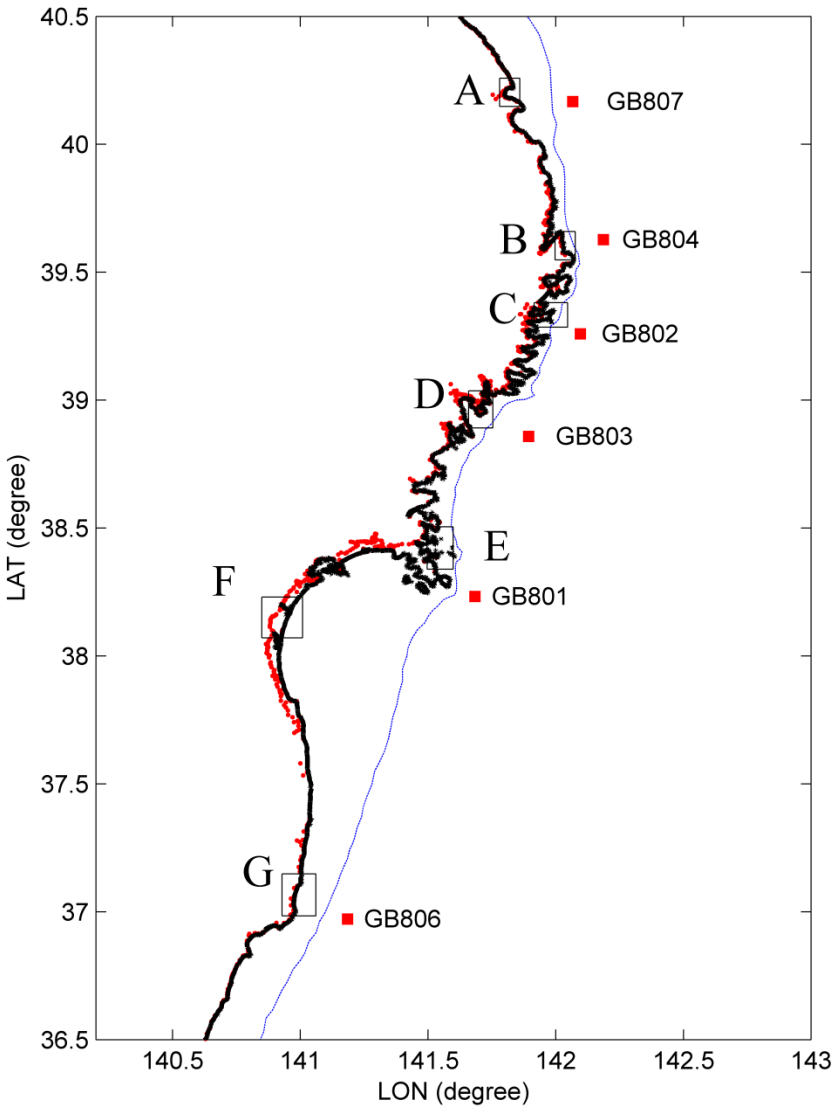

Fig. 7: The eastern Japan coastline with surveyed run-up points (dots) from 2011 Tohoku Earthquake Tsunami Joint Survey (TTJS) Group, location of GPS buoy data from NOWPHAS (squares), regions for the run-up height comparison (open rectangles), and a 100 m water depth contour from mean high water level (thin line).

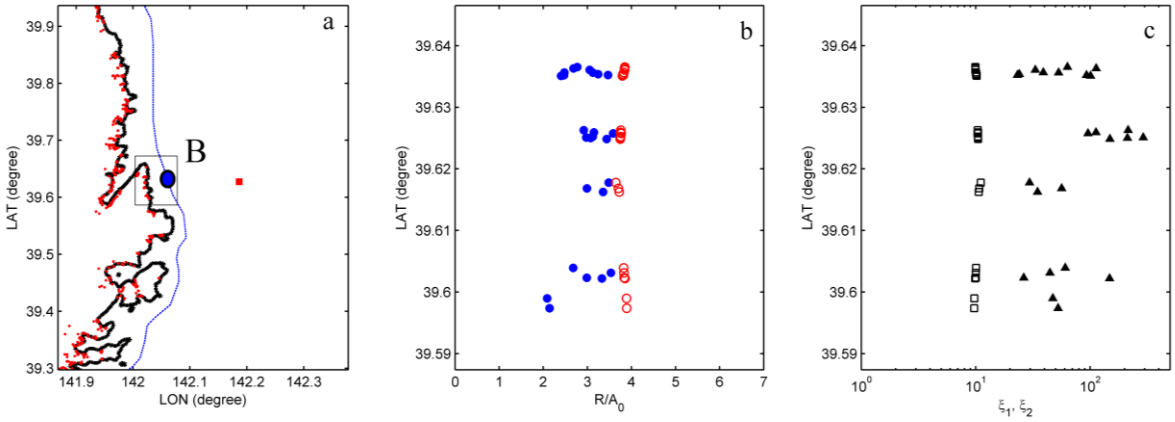

Fig. 8: Run-up height comparison results for Region B. (a) Coastline map with 100 m water contour (thin line), location of 100 m water depth for model input (solid circle), and GPS buoy location (solid square). (b) Comparison of the relative run-up heights from the survey (solid circle) and the new equation (open circle). (c) ξ_1 and ξ_2 values (open squares and solid triangles).

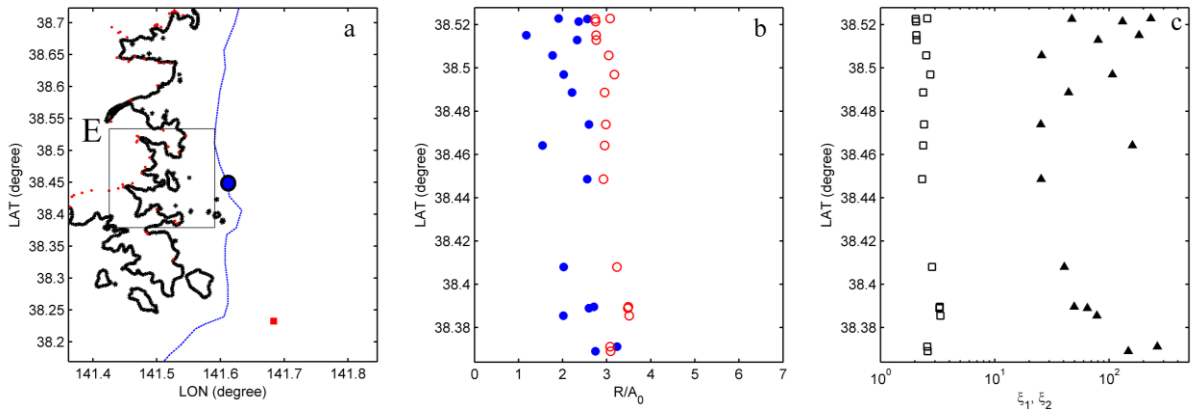

Fig. 9: Run-up height comparison results for Region E. Symbols are same as Fig. 8.

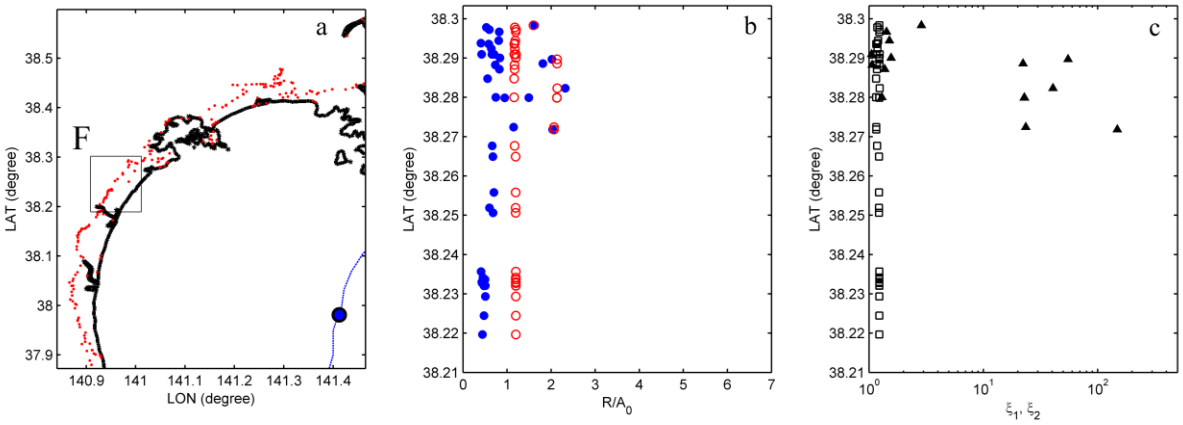

565

566 Fig. 10: Run-up height comparison results for Region F. Symbols are same as Fig. 8.
567

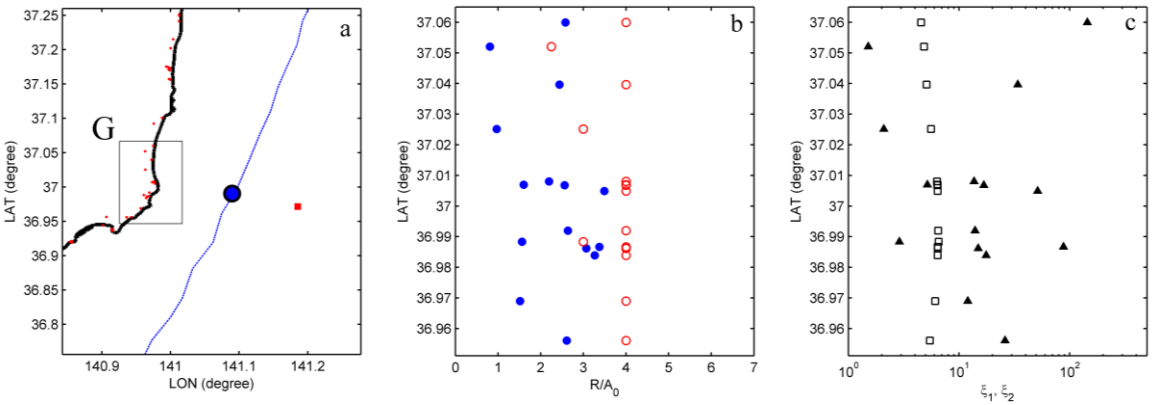

568

569 Fig. 11: Run-up height comparison results for Region G. Symbols are same as Fig. 8.

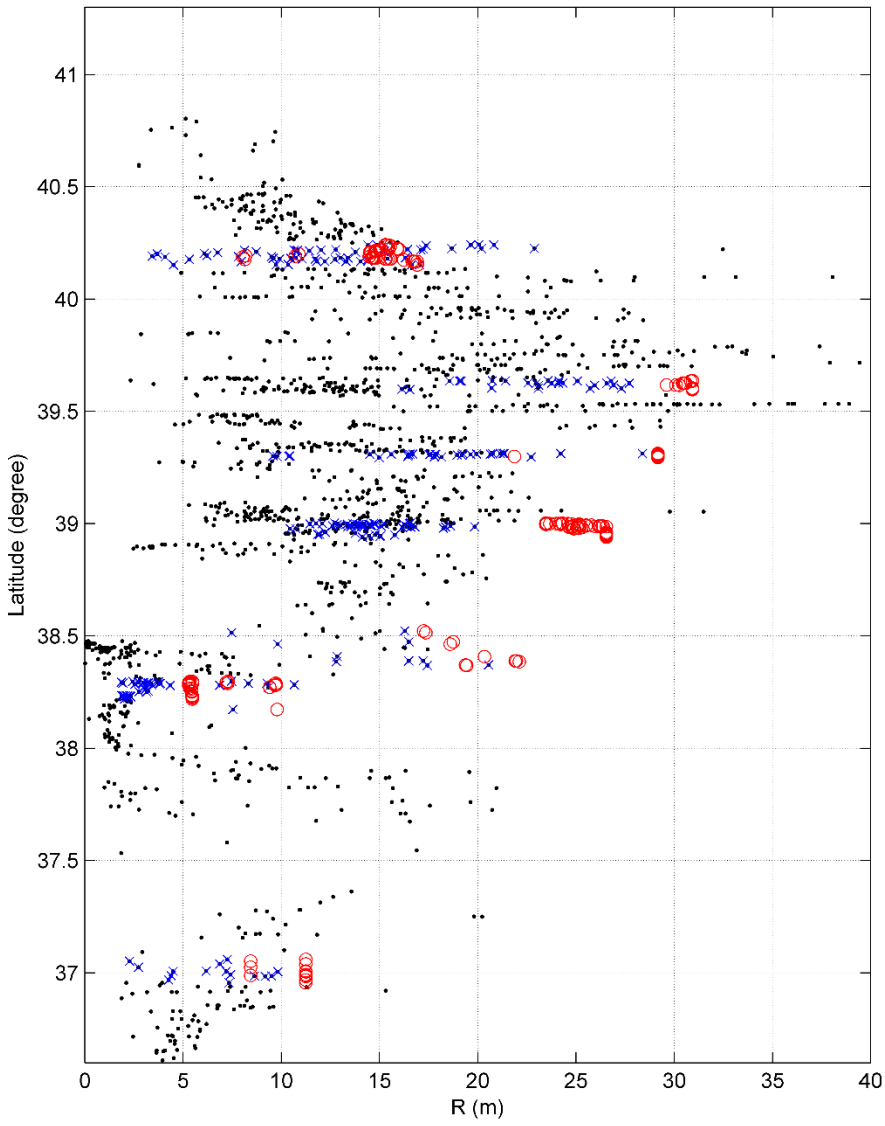

570

571 Fig. 12: Total surveyed run-up heights (dots) along the coastline from 36.5˚N to 41˚N,
572 surveyed data used for comparison (cross marks), and corresponding Eq. 10 estimates (open
573 circles).

574 **List of Tables**

577

578 Table 1: Detail GPS Buoy Data in 2011 Tohoku Tsunami, Japan

Buoy	Location	Distance (km)	h_{buoy} (m)	A_{buoy} (m)	H_{buoy} (m)	T (s)	A_{buoy}/h_{buoy} (-)
GB807	40°07′00″ 142°04′00″	20.6	125	4.0	4.5	1100	0.032
GB804	39°37′38″ 142°11′12″	14.5	200	6.5	8.2	1200	0.033
GB802	39°15′31″ 142°05′49″	17.2	204	6.1	9.4	1510	0.030
GB803	38°51′28″ 141°53′40″	25.5	160	5.9	8.9	1000	0.037
GB801	38°13′57″ 141°41′01″	30.9	144	5.8	10.8	1400	0.040
GB806	36°58′17″ 141°11′08″	20.1	137	2.6	2.7	1250	0.019

579

580 Table 2: Surveyed data for the model comparison.

SITE	A_0 (m)	$Dist_1$ (km)	$Dist_2$ (m)	T (s)	$Cot(\beta_1)$ MEAN (STD)	ξ_1 MEAN (STD)	$Cot(\beta_2)$ MEAN (STD)	ξ_2 MEAN (STD)
A	4.2	13.0	300	1100	130 (14.4)	4 (0.5)	46 (123.2)	132 (114.0)
B	7.7	3.7	160	1200	37 (1.2)	11 (0.3)	7 (4.7)	149 (154.3)
C	7.3	10.0	410	1510	100 (6.1)	5 (0.3)	28 (36.1)	161 (372.8)
D	6.6	8.4	210	1000	84 (11.7)	4 (0.7)	15 (14.3)	105 (140.0)
E	6.4	19.7	120	1400	197 (31.3)	3 (0.4)	8 (6.1)	142 (105.7)
F	4.6	44.3	2,200	1250	443 (12.0)	1 (0.0)	896 (723.2)	13 (35.9)
G	2.8	11.9	390	1100	112 (14.3)	6 (0.7)	96 (128.3)	42 (55.3)

581